Chinese Chemical Letters 34 (2023) 108071

Contents lists available at ScienceDirect

Chinese Chemical Letters

journal homepage: www.elsevier.com/locate/cclet

Vanillin cross-linked hydrogel membranes interfacial reinforced by carbon nitride nanosheets for enhanced antibacterial activity and mechanical properties

Umer Shahzad Malik[a,1], Qixiang Duan[b,1], Muhammad Bilal K. Niazi[a,*], Zaib Jahan[a], Usman Liaqat[a], Farooq Sher[c], Yanchang Gan[b,*], Honghao Hou[b,*]

[a] School of Chemical and Materials Engineering, National University of Sciences and Technology, Islamabad 44000, Pakistan
[b] Guangdong Provincial Key Laboratory of Construction and Detection in Tissue Engineering, School of Basic Medical Science, Southern Medical University, Guangzhou 510515, China
[c] Department of Engineering, School of Science and Technology, Nottingham Trent University, Nottingham NG11 8NS, United Kingdom

ARTICLE INFO

Article history:
Received 18 July 2022
Revised 12 December 2022
Accepted 12 December 2022
Available online 14 December 2022

Keywords:
Green synthesis
Sustainable membranes
Starch capped silver nanoparticles
g-C_3N_4 nanosheets
Wound dressing
Antibacterial

ABSTRACT

Biopolymer based hydrogels are highly adaptable, compatible and have shown great potential in biological tissues in biomedical applications. However, the development of bio-based hydrogels with high strength and effective antibacterial activity remains challenging. Herein, a series of vanillin-cross-linked chitosan nanocomposite hydrogel interfacially reinforced by g-C_3N_4 nanosheet carrying starch-caped Ag NPs were prepared for wound healing applications. The study aimed to enhance the strength, sustainability and control release ability of the fabricated membranes. Starch-caped silver nanoparticles were incorporated to enhance the anti-bacterial activities The fabricated membranes were assessed using various characterization techniques such as FT-IR, XRD, SEM, mechanical testing, Gel fraction and porosity alongside traditional biomedical tests *i.e.*, swelling percentage, moisture retention ability, water vapor transmission rate, oxygen permeability, anti-bacterial activity and drug-release of the fabricated membranes. The mechanical strength reached as high as 25.9 ± 0.24 MPa for the best optimized sample. The moisture retention lied between 87%–89%, gel fraction 80%–85%, and water vapor transmission up to 104 ± 1.9 g m^{-2} h^{-1} showing great properties of the fabricated membrane. Swelling percentage surged to 225% for blood while porosity fluctuated between 44% ± 2.1% and 52.5% ± 2.3%. Oxygen permeability reached up to 8.02 mg/L showing the breathable nature of fabricated membranes. The nanocomposite membrane shown excellent antibacterial activity for both gram-positive and gram-negative bacteria with a maximum zone of inhibition 30 ± 0.25 mm and 36.23 ± 0.23 mm respectively. Furthermore, nanoparticles maintained sustainable release following non-fickian diffusion. The fabricated membrane demonstrated the application of inorganic filler to enhance the strength of biopolymer hydrogel with superior properties. These results envisage the potential of synthesized membrane to be used as wound dressing, artificial skin and load-bearing scaffolds.

In the face of medical and healthcare science, wound healing is one of the major challenges [1]. Wounds are highly vulnerable to bacterial infections causing serious complications and dissemination of bacterial invade. Laceration healing is a complex process involving various types of growth factors, vitamins, cytokines, minerals and cells [2]. The wound healing process has been divided into four different overlapping phases which are hemostasis, inflammation, proliferation and remodeling [3]. The inflammation stage is vulnerable to bacterial infection and can lead to serious damages such as tissue damage, followed by proliferation where fibroblast proliferation occurs which is necessary for wound granulation [4]. Therefore, wound must be covered with some efficient dressing to treat these various stages of healing.

Currently, efforts are dedicated to fabricate novel dressings to improve the wound healing. Among various dressings, such as sponge, gel, hydrocolloid, and fiber, hydrogels based on bio-origin have received central attraction owing to their excellent biocompatibility, biodegradability, high water content and high oxygen

* Corresponding authors.
E-mail addresses: m.b.k.niazi@scme.nust.edu.pk (M.B.K. Niazi), ganyanzhang@163.com (Y. Gan), ss.hhh89@hotmail.com (H. Hou).
[1] These authors contributed equally to this work.

https://doi.org/10.1016/j.cclet.2022.108071
1001-8417/

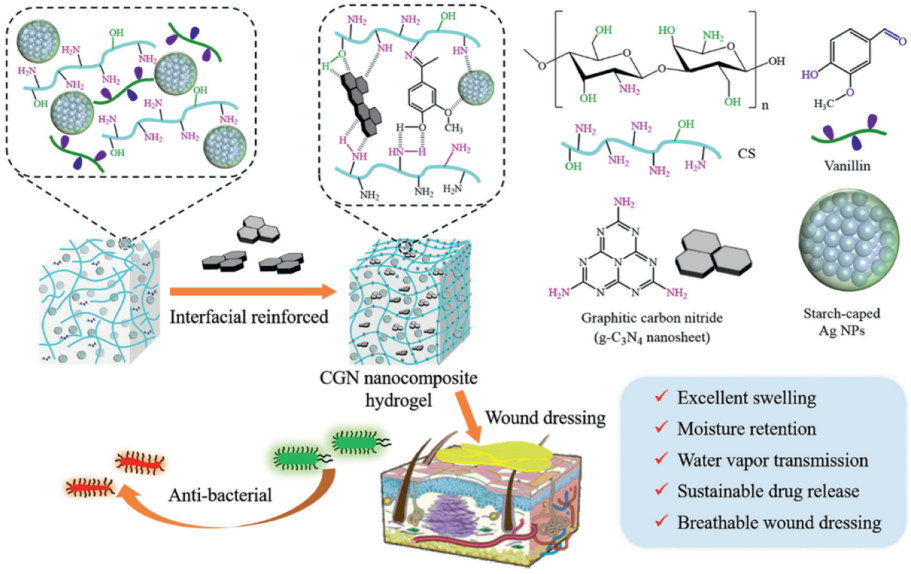

Fig. 1. Schematic synthetic process of chitosan/vanillin/GCN/AgNPs nanocomposite hydrogel membranes with enhanced antibacterial activity potential for application in wound healing.

permeability, which resemble the features of extracellular matrix (ECM) [5]. Therefore, hydrogel membranes could be considered ideal candidates for wound dressings [6]. Chitosan, a biomedical material has excellent properties such as non-toxicity, antimicrobial properties, biodegradability, and biocompatibility and it is one of the most used polymer in hydrogels, especially for wound dressings [7]. Besides the bulk biomaterial, suitable nontoxic and natural polymer cross-linkers are another key to prepare green and sustainable hydrogels. Vanillin, a primary extract of vanilla bean is widely used in pharmaceuticals, cosmetics, foods and beverages, it has one aldehyde and one hydroxyl group in its structure making it active cross-linker [8].

Despite much progress for positive therapeutic effects on wound healing, the applications of bio-based hydrogels wound dressings are limited due to relatively low mechanical properties [9]. The mechanical weakness of conventional hydrogels not only makes it difficult to peel off wound beds when they are refreshed but also severely restricts their application as load-bearing scaffolds. Therefore, a lot of research is being conducted to overcome the strength issue such as many natural and synthetic polymers are blended in hydrogel-membranes to make it robust [2]. Organic-inorganic membranes are one of these blends where inorganic fillers are embedded into polymeric matrix, such as zeolite immendazolite frameworks (ZIF) [10], graphene oxide (GO) [11], mesoporous silica [12] and carbon nanotubes (CNTs) [13]. Graphitic carbon nitride (g-C_3N_4), as an emerging, metal-free semiconductor material with a two-dimensional (2D) lamellar structure have been explored for a wide variety of applications owing to their unique properties, such as their large specific surface area, good electrical performance and high photoactivity [14]. Notably, its superior mechanical properties and high thermal stability suggest that it can be used to enhance the poorly mechanical properties of bio-hydrogels [15]. More importantly, g-C_3N_4 nanosheets can offer outstanding antibacterial properties, potential photothermal therapy, and fluorescent imaging properties for versatile biomedical applications [16]. To unleash their biomedical applications, g-C_3N_4 need to be prepared with various architectures without changing their intrinsic attributes. Considering all these aspects of g-C_3N_4 it is feasible to employ it as an effective filler to enhance the mechanical properties of bio-polymer based wound dressing membranes.

Nonetheless advancement in wound management, morbidity caused by infections is a considerable issue. That is why research is still underway to counter this problem. Up till now, considerable efforts have been devoted to antibacterial hydrogels carrying drugs, metal ions, and inorganic nanoparticles and so on. Silver nanoparticles (AgNPs) have been known to be effective antibacterial agents for a long time, and their toxicity has been further reduced using silver-binding membranes [17]. Furthermore, these nanoparticles have antibacterial properties against a wide range of viruses, fungi and bacteria [18]. Safer and green routes for the synthesis of Ag NPs have been extensively reported recently, which not only make them environment friendly but also reduce the cytotoxicity [19]. Hence, as shown in Fig. 1, the incorporation of these particles in biopolymers has become a new interest in the said area. Acknowledging the superior properties and potential for biomedical applications of the above discussed materials, herein vanillin-cross-linked chitosan/starch-caped Ag NPs nanocomposites hydrogel membranes reinforced by g-C_3N_4 nanosheets were developed for wound dressing. The starch-caped silver-nanoparticles (AgNPs) fabricated through green one-pot method were incorporated into the hydrogels to enhance the antibacterial activities. The solution casting method was employed to fabricate nano-composite hydrogel membranes consisting of chitosan-vanillin, g-C_3N_4 and starch caped silver nanoparticles (Table S1 in Support information). The g-C_3N_4 was used as filler to increase strength along with AgNPs. The obtained nanocomposite membranes were evaluated through Fourier transform infrared spectroscopy (FT-IR), X-ray diffraction (XRD), scanning electron microscopy (SEM), tensile strength, compressive strength. Different biological tests were also conducted such as swelling percentage, moisture retention ability, water vapor transmission rate, oxygen permeability, anti-bacterial activity and drug-release behavior of the synthesized membranes. This novel and functional nanocomposite hydrogel could be used as an ideal candidate material for wound dressing or load-bearing scaffold.

The FT-IR spectra of g-C_3N_4, AgNPs and nanocomposite membranes are depicted in Figs. 2a and b and Fig. S1 (Supplementary material). There are five characteristics peaks of g-C_3N_4 in the range 1200–1700 cm^{-1} region attributed to the stretching of CN heterocycles (C=N, C–N) (Fig. 2a). The peak at 812 cm^{-1} is the typical triazine unit breathing [20]. In the FT-IR spectrum of

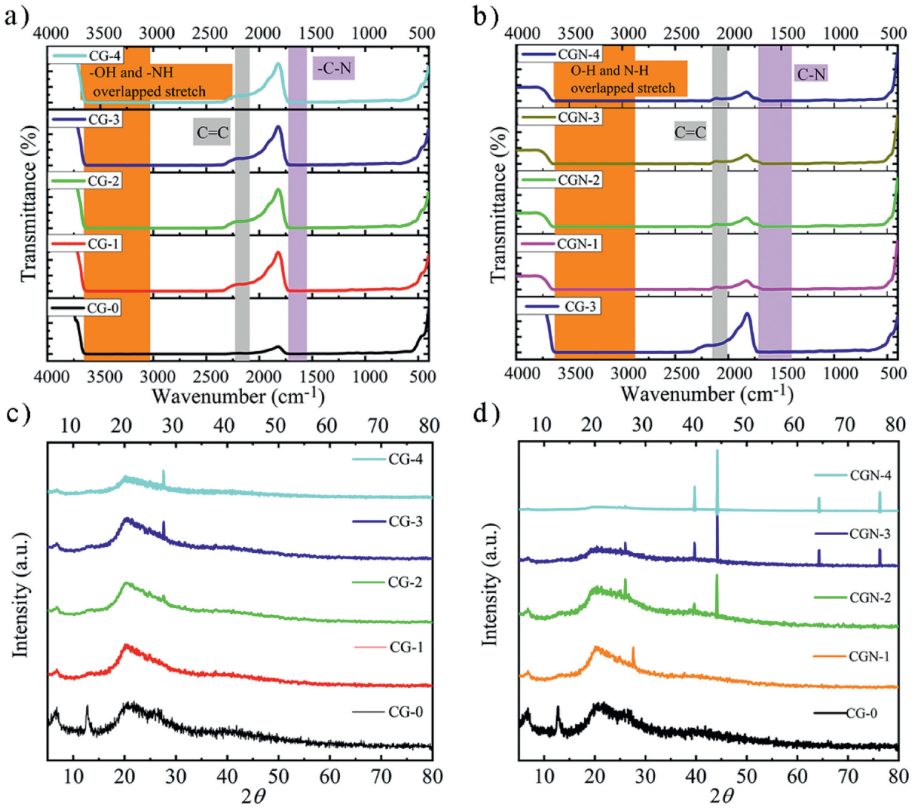

Fig. 2. (a, b) FT-IR spectra and (c, d) XRD pattern of (a, c) chitosan/vanillin/GCN and (b, d) chitosan/vanillin/GCN/AgNPs.

starch-caped silver nanoparticles (Fig. 2b), the wide stretched peak at 3400 cm^{-1} is the characteristic peak of starch, the peak at 2935 cm^{-1} is the -C-H stretching while O–H stretching can be seen at 1635 cm^{-1}. Other peaks like 1440 cm^{-1} are concerned with the bending vibrations of -C-H and CH_2. The peaks in fingerprint region like 878 cm^{-1} and below are due to the C–O-C ether stretching vibrations [21]. Different interactions developed between components of hydrogels during fabrication, however, due to the similar composition, the spectrum of composite membranes looked alike. As shown in Figs. 2a and b, broad peak around 3400 cm^{-1} shows the great number of -O-H functional groups present in starch, chitosan, and in vanillin and -NH overlapping. The peak at ~1650 cm^{-1} shows the formation of Schiff base bonds between carbonyl groups of vanillin and NH_2 groups of chitosan [22]. Massive hydrogen bonds occurred between -OH groups of chitosan, vanillin, and starch from nanoparticles which is evident from the intense broad peaks at around 3400 cm^{-1} [23], similar results were reported by Hu *et al.* [24,25].

The XRD analysis of g-C_3N_4, AgNPs and composite membranes was conducted to study the phase analysis and crystal structure (Figs. 2c and d, and Fig. S2 in Supporting information). The XRD pattern of g-C_3N_4 depicts two characteristics peaks (Fig. S2a), the stronger one at 27.35° is indexed as (002), which is due to the conjugated aromatic planes interlayer stacking. The d-space for this peak is 0.325 nm. The weaker peak at 12.85° is indexed as (100), which is due to the plane structural packing motif of tri-*s*-triazine units [20]. The d-spacing for this peak is 0.693. The crystalline size of g-C_3N_4 is 8.4 nm that is calculated by Debye-Scherrer equation. The XRD pattern of starch capped silver nanoparticles depicted four characteristic peaks identified at 2θ 38.1°, 44.1°, 64.5° and 76.8° (Fig. S2b). The crystal planes corresponding to above peaks are (111), (200), (220) and (311), respectively [26]. The average crystalline size was calculated using Debye-Sherrer's equation and found to be 42 nm. The reposted values agree with the (JCPDS No. 04–0783) and matched FCC lattice.

The XRD pattern of composite membranes shown various characteristic peaks of their constitutes as reported in Figs. 2c and d. In CG-0, three peaks are clearly visible at 20°, 12° and ~6°. The peak at ~20° shows the characteristic peak of chitosan, while the sharper peak at ~12° is characteristic peak of vanillin showing its crystalline nature [27]. Vanillin cross-link chitosan can be identified by peaks at ~6.8° and ~13°, which exposes the intermolecular interactions between both polymers [28]. While in CG-1 composite membrane, the vanillin peak disappeared which can be attributed to the bonding between g-C_3N_4 and vanillin. Moreover, no peak for g-C_3N_4 is observed showing its consumption in a chemical reaction between chitosan and vanillin and good dispersion into the polymer matrix, as reported by Inagabire *et al.* [29] in their work as well. In the next diffraction pattern, CG-2, a little spike at around ~26° is observable that can be attributed to the g-C_3N_4 presence in the composite membrane. This peak can be seen dominating in the next two diffraction patterns, showing that g-C_3N_4 accumulated in the composite hydrogel. Fig. 2d depicts the XRD pattern of chitosan/vanillin/GCN/AgNPs hydrogel membrane. From bottom to top, emerging peaks of silver nanoparticles at their featuring positions are observed such as at ~38°, ~44°, ~64° and ~76° [30] confirming the well embodiment of nano-particles in hydrogel membrane, Wu *et al.* [31] observed similar results.

Surface morphologies of the chitosan/vanillin/GCN/AgNPs sample were observed by SEM (Fig. S3 in Supporting information). As expected, the composite hydrogel membranes shown dense structure without any apparent pores up to 10,000 magnifications and the surface of clean chitosan/vanillin is homogenous and smooth authenticating the great miscibility of both components in each other. However, as the concentration of g-C_3N_4 increased the agglomerations were visible. The composites with various concen-

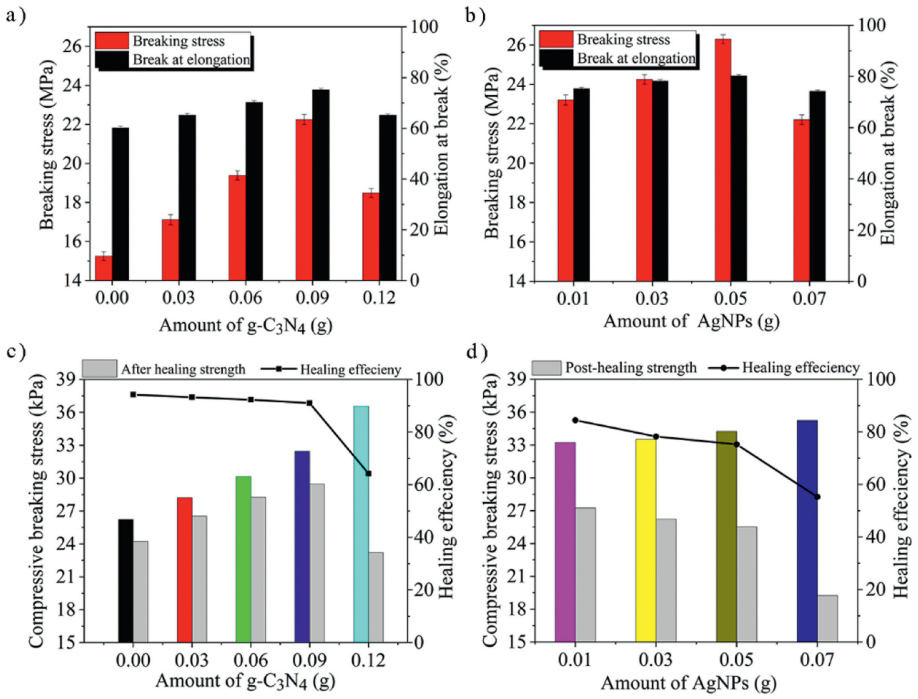

Fig. 3. Mechanical strength and elongation at break of (a) chitosan/vanillin/GCN, (b) chitosan/vanillin/GCN/AgNPs and self-healing properties of (c) chitosan/vanillin/GCN and (d) chitosan/vanillin/GCN/AgNPs nanocomposite membranes.

trations of nanoparticles shown dense morphologies, which is favorable in wound dressing applications as no microbes can enter through the polymer matrix. Looking at the 0.1 g of AgNPs, the surface looks compact and homogenous showing the complete dissolution and smooth spread of nanoparticles in the polymeric chain. However, an increasing amount came up with agglomerations of nanoparticles over the surface, due to the high surface energy of nanoparticles it formed chunks. The cross-section images of fabricated membranes shown no pores or cracks (Fig. S4 in Supporting information).

The porosity plays important role in absorption of exudates and enhanced surface area. It also helps in the diffusion of fluids inside membranes and facilitates functional groups interaction with coming fluids. Table S2 (Supporting information) is presenting the porosity and density of composite membranes, in porosity, trends are decreasing with increasing content of g-C_3N_4 reaching maximum porosity of 52.5 ± 2.3 for CG-1 to lowest at 44.6 ± 2.4 for CG-4. The reasons for this decreasing trend are due to the compaction of the membrane with increasing filler eventually causing pore fills as per concluded from SEM results. The highest pores were noticed for low filler quantity. The porosity increased when the quantity of NPs content increased. The increasing trend may be due to the chain enlargement of the polymer matrix [19].

In wound dressing applications, one of the most important parameters for dressing material is their mechanical strength and break at elongation. Hence, the membranes must endure the harsh environment and remain intact and useful during the service [32]. Herein, incorporation of filler g-C_3N_4 as expected significantly improved the mechanical strength and elongation at break of the fabricated membranes. As shown in Fig. 3 with an increase of g-C_3N_4 filler from 0.03 g to 0.09 g, the mechanical strength improved from 15.25 ± 0.21 MPa to 22.25 ± 0.26 MPa while flexibility increased from 60.24% to 75.2% (highest) respectively, showing great interfacial interactions between the polymeric elements and inorganic filler. The highest achieved strength was 22.25 ± 0.26 MPa with an increase of 145% from the pristine sample. The enhancement can be credited to the interfacial interactions and good dispersion of organic filler in the polymer matrix such as reported by Yang *et al.* [33,34]. The improvements can also be credited to the excessive hydrogen bonding in the matrix. However, the strength and elongation at break decreased rapidly from 0.09 g to 0.12 g of filler incorporation. This rapid decrease can be justified by the deterioration of the matrix inner lamellar structure due to filler accumulation as explained by Fan *et al.* [35]. While the reduction in the flexibility from CG-3 to CG-4 might be because of an upsurge of susceptibility and decreased degree of entanglement. Another possible reason can be the high degree cross-linking which might have reduced the mobility of the polymeric matrix significantly. However, looking from a broader angle, the strength increase was dominant and clearly noticeable from blank hydrogel to hydrogel with 0.09 g of g-C_3N_4. That is why this sample, CG-3 was chosen to be incorporated with nanoparticles.

The addition of NPs from 0.01 g to 0.05 g not just enhanced the stress endured from 23.21 ± 0.19 MPa (CGN-1) to 25.9 ± 0.24 MPa (CGN-3) but the elongation as well from 76.25% ± 2.1% (CGN-1) to 80.25% ± 1.9% (CGN-3). Hence NPs in the composition can be ascribed as the secondary reinforcement. The strength enhancement can be attributed to the uniform distribution of AgNPs in the polymeric matrix, the interfacial contact with the polymer and the expected bonding between polymer and NPs [36,37]. The tight mesh structure can be given credit to the mechanical enhancement as well [37]. However, further increase of AgNPs lower down the mechanical strength and elongation to 22.21 ± 0.23 MPa and 75.21% for CGN-4 respectively. The reason might be due to the compact structure, more bonding, or accumulation of particles on the surface [38]. Figs. 3c and d represents the self-healing efficiency of fabricated membranes using the compressive strength method, on increasing contents of filler the healing efficiency slightly reduced from 94.12% to 91.23% for CG-1 to CG-3 respectively which is a negligible difference. The healing properties can be attributed to the Schiff base bond formation between -CHO group of vanillin and -NH_2 group from chitosan and g-C_3N_4 as evident from FT-IR results. The results show that nano-filler not just helped in increasing strength but also helped in maintaining self-healing properties

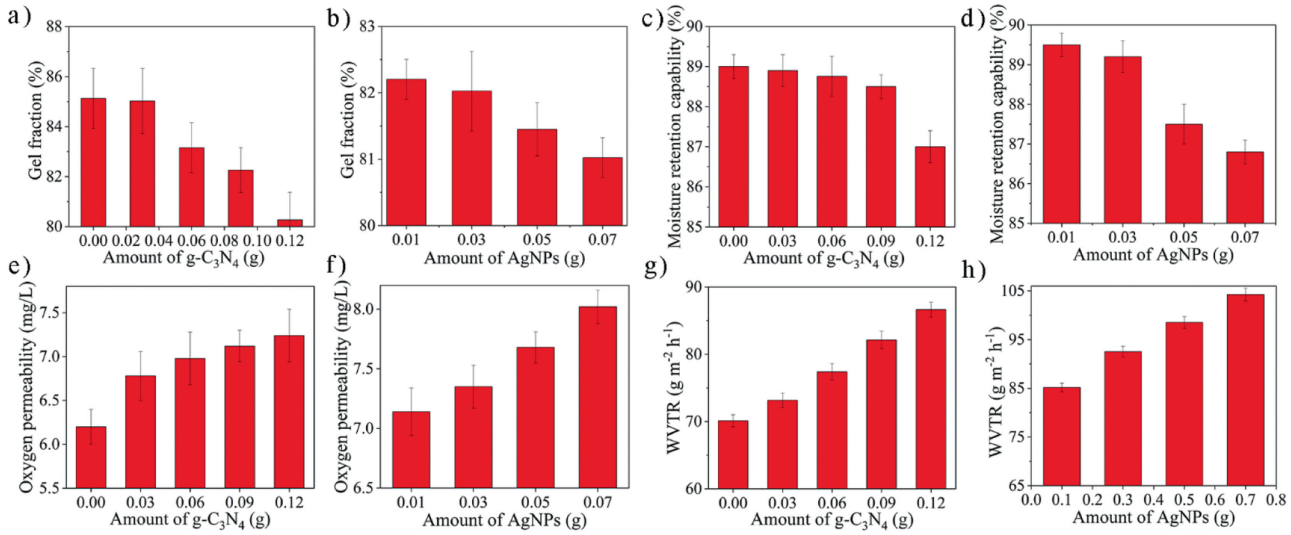

Fig. 4. Gel fraction of (a) chitosan/vanillin/GCN, (b) chitosan/vanillin/GCN/AgNPs and moisture retention capabilities of (c) chitosan/vanillin/GCN and (d) chitosan/vanillin/GCN/AgNPs nanocomposite membranes. Oxygen permeability of (e) chitosan/vanillin/GCN, (f) chitosan/vanillin/GCN/AgNPs. Water vapor transmission rate of (g) chitosan/vanillin/GCN and (h) chitosan/vanillin/GCN/AgNPs.

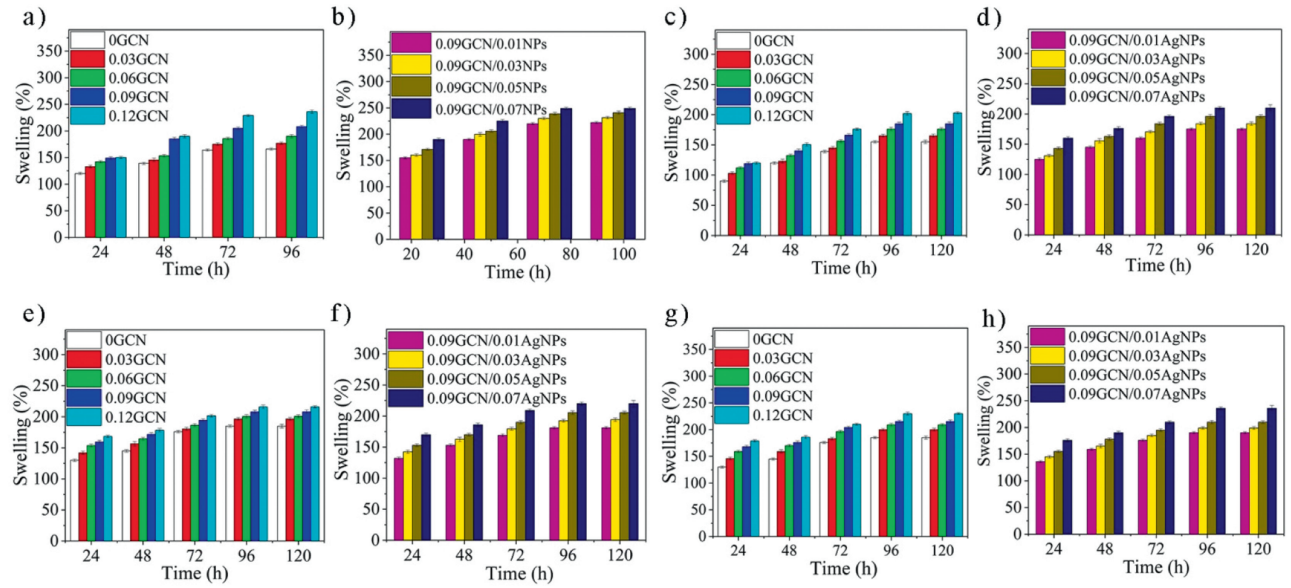

Fig. 5. Swelling percentages of chitosan/vanillin/GCN in (a) Water, (c) Salt, (e) Blood and (g) Simulated wound fluid and chitosan/vanillin/GCN/AgNPs hydrogel in (b) Water, (d) Salt, (f) Blood and (h) Simulated wound fluid sequentially.

[39]. However, self-healing abilities rapidly reduced from CG-3 to CG-4. These results indicated that further increase of filler hindered the self-healing phenomenon. The reduction in healing efficiencies can be attributed to filler accumulation, network compaction, and massive bonding upon increasing filler quantity. The same trends continued in Fig. 3d where upon increasing NPs in the membrane, the compressive strength increased with decreased healing efficiency. The addition of more NPs hindered the healing efficiency, the heating efficiency for sample CGN-1 to CGN-3 decreased from 84.45% to 75.9%, this may be due to the hydrogen bonding prevalence over Schiff base bonding, similar conclusion was drawn by Talodthaisong *et al.* [40].

Gel fraction (GF) accesses the efficiency of cross-linker in fabricated membranes. Gel fraction values lie in the 80–85% range for different g-C_3N_4 amounts in chitosan/vanillin/GCN composite (Figs. 4a and b). From left to right the GF value slightly decreased, from 85.124 (CG-0), the highest, to 80.26 (CG-4), the lowest. The filler reduced the value which may be because of polymer entanglement decreased by increasing amounts of filler as per Yokoyama *et al.* [41]. However, overall good values of GF show the effectiveness of vanillin as a cross-linker. With NPs introduction, the gel fraction values decreased as well as noticed in Fig. 4b. This may be due to the expansion of the membrane and corresponds to less crosslinking. The decline can also be attributed to the interactions of AgNPs with -NH_2 and -OH functional groups *via* hydrogen bonding. The decrease may also correspond to the hydrophilic nature of filler and starch-caped silver nanoparticles [42]. The GF reduction value facilitates the release of AgNPs from the polymeric matrix and enhances the wound healing phenomenon [43].

The moisture retention capabilities are related to the property of hydrogel membranes through which they demonstrate the loss of water. This property regulates the process through which the

membranes interact with the wounds and effects the adsorption properties. Hydrogels are known to exhibit a large quantity of water in their hydrophilic matrices. Moist the wound, easier will be the wound healing phenomenon [44]. Moisture retention capabilities are shown in Figs. 4c and d. The moisture retention values of all samples lie in the range of 87% to 89% showing insignificant deviations similar to previous conclusions by Wen-Chun *et al.* [31]. This good moisture retention ability of the membrane can be credited to the excessive -OH bonds in the polymeric matrix, while g-C_3N_4 is also hydrophilic. The water is locked in the compact structure and hardly escape from the entangled networks. High moisture retention values are preferred for the materials expected to be used in wound dressing applications. This is due to the fact that moist environments are mean to be wound healing accelerators and tissue repairing [45].

The oxygen permeability was measured for fabricated membranes using dissolved oxygen as a parameter by adopting the method reported in the literature [46]. With a flask, divalent manganese solution was made followed by adding sodium hydroxide (NaOH) in it which swiftly oxidized Mn^{2+} valency, following this method dissolved oxygen (DO) quickly oxidized into equal amount as of divalent manganese ions (Mg^{2+}). Afterwards, Potassium iodide (KI) was added to acidify the solution. Consequently, free iodide ions were produced with an equal amount as of DO. Water was titrated using sodium thiosulphate solution (0.025 N). Blue point indicated the endpoint using starch as an indicator. For an open bottle, the value of dissolved oxygen is 12.60 mg/L and 6 mg/L for closed bottle. The bottles covered with composite membranes shown DO between 6.2 ± 0.23 to 8.02 ± 0.4 mg/L. The results (Figs. 4e and f) shown promising values compared with a closed bottle and indicated the competency of fabricated composite membranes, the highest oxygen permeability was noticed against CGN-4 (8.02 mg/L). The results further indicated that fabricated membranes could be used as wound dressing materials due to their breathable nature.

The water vapor transmission rate (WVTR) of fabricated membranes is illustrated in Figs. 4g and h. The WVTR of g-C_3N_4 with different amounts is shown where increasing trends can be noticed (Fig. 4g). The negative control is a sealed bottle while the positive control is an open bottle with WVTR as 380.2 g m^{-2} h^{-2}. However, it can be observed that once the bottles were covered with membranes, the vapor transmission rate was greatly reduced. The WVRT for CG-1, CG-2, CG-3 and CG-4 were 70.115, 73.152, 77.413, 82.156 and 86.64 g m^{-2} h^{-1} respectively. These results are evident that the membranes are enough to act as a barrier in way of transmission and can strictly prevent water loss from the wound. The increasing rate of water vapor transmission rate can be attributed to the introduction of hydrophilic filler, similar trends were observed by Achachlouei *et al.* [47] When the composite membranes were loaded with NPs as illustrated in Fig. 4h, the trend remained the same *i.e.*, increasing, with maximum values at 98 ± 2.1 g m^{-2} h^{-1} and 104 ± 1.9 g m^{-2} h^{-1} for CGN-3 and CGN-4, respectively. This might be because nanoparticles helped in matrix enlargement and due to the hydrophilic nature of nanoparticles as well. Zhang *et al.* [48] found the same trends with their figures lying between 82 and 98 g m^{-2} h^{-1}. The optimum conditions for water vapor transmission in wound management are 92–190 g m^{-2} h^{-1}. Hence, the fabricated hydrogels are potential candidates for wound healing materials.

The knowledge of swelling behavior of a material is very important in the pharmaceutical and biomedical applications. In the present study, the swelling of hydrogel membranes was tested against distilled water, 0.9% NaCl, blood and simulated wound fluid (SWF) (Fig. 5). In water (Figs. 5a and b), the swelling reached high percentages *i.e.*, 230% for CGN-3 (96 h), due to the presence of hydrophilic functional groups. The trends have shown

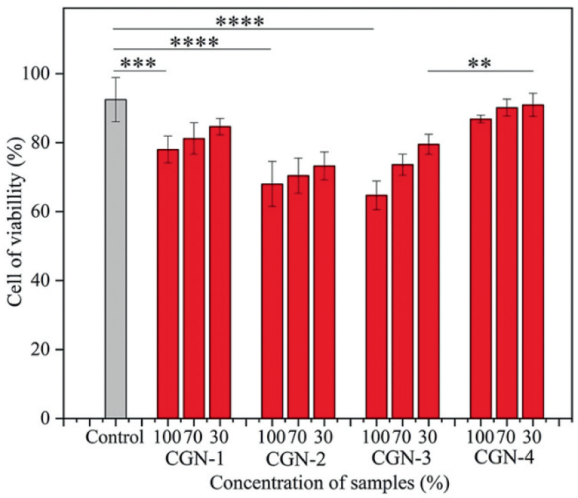

Fig. 6. Graphical presentation of cytotoxicity evaluation of fabricated chitosan/vanillin/GCN/AgNPs membranes (**$P < 0.01$, ***$P < 0.001$, ****$P < 0.0001$).

that cross-linking degrees are directly dependent upon swelling, as the value of crosslinking decreased, the swelling improved. Achachlouei *et al.* [47] reached to the same conclusions. The same trends were observed in both chitosan/vanillin/GCN and chitosan/vanillin/GCN/AgNPs. The addition of AgNPs further improved the swelling properties as NPs have charged species which facilitates the water absorption. Furthermore, the AgNPs created spaces that were filled with water. The great swelling percentages can also be ascribed to the hydrogen bonding formation between the molecules of water and -OH functional groups. The swelling percentages were lower in salt water in comparison with the distilled water (Figs. 5c and d), the maximum value reached in this case was ~200% for CG samples and ~210% for CGN-3 (96 h). This comparison is in well agreement with Çay *et al.* [49]. The expected reasons can be explained by that electrostatic repulsion may have blocked the polymeric chain accumulation and expanded the network [50]. In blood (Figs. 5e and f, the maximum swelling percentages were higher compared to both previous media *i.e.*, 168.5%, 178.5%, 201.5%, 216% and 218% for CG-0, CG-1, CG-2, CG-3 and CG-4 respectively. For CGN samples swelling ratios were 170%, 186%, 209%, 220% and 225% respectively from CGN-1 to CGN-4 respectively. The great swelling in the blood may be credited to various reasons, such as the crosslinking might have intensified the molecular space eventually destroying the hydrogen bonding concluded by Biranje *et al.* as well [51]. The ionic nature of blood also enhances the electroneutrality effect which creates additional osmotic pressure inside the polymeric matrix [52]. Likewise, the swelling in simulated wounds shown tremendous swelling percentages as shown in Figs. 5g and h, the reasons are obvious from blood and NaCl solution. These results have suggested that this hydrogel membrane is capable of accumulating and absorbing fluids from wounds. The ideal range for swelling percentage should fall within 100%–900% range [51], hence fabricated membranes have encouraging results to be used as wound dressing materials for granulating wounds.

The MTT assay helped us to determine the safety profile of chitosan/vanillin/GCN/AgNPs membranes. The assay revealed that cells treated with synthesized membranes showed high cellular viability. Based on the experimented results of cytotoxicity all samples exhibited proliferative activity against HEK-293 cells (Fig. 6). For CGN-3 to CGN-4 the cell viability increased from 79.53% to 90.95% against 30% concentration. The previous studies have also shown the nontoxic nature of starch-caped silver nanoparticles,

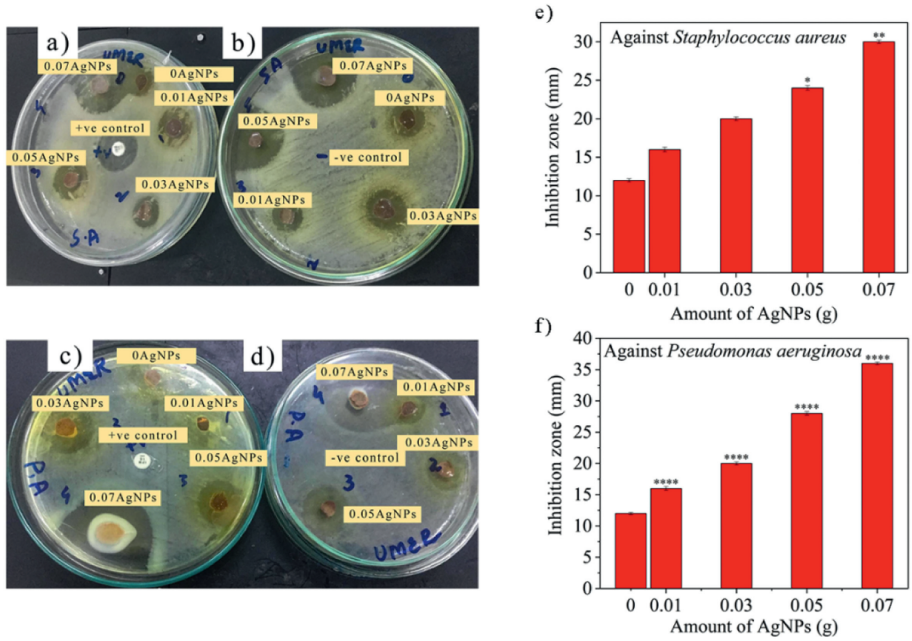

Fig. 7. Representation of Kirby-Bauer agar plates of (a, b) *S. aureus*, (c, d) *Pseudomonas aeruginosa* and graphical representation of zone of inhibition of (e) *S. aureus* and (f) *Pseudomonas aeruginosa* ($^{*}P < 0.05$, $^{**}P < 0.01$, $^{****}P < 0.0001$).

this may be due to the capping of starch which inhibits silver ions release and serves as protective layer [53]. Therefore, based on the observed results it is safe to envisage the CGN membranes as promising dressing material for wounds.

The bacterial activity of developed membranes was measured using disk diffusion method against Gram-negative *Pseudomonas aeruginosa* and Gram-positive *Staphylococcus aureus*. Clear inhibition zones formed around hydrogels showing great activity against both bacterial strains as shown in Figs. 7a-d. An increase in activity was noticed with increased contents of AgNPs (Figs. 7e and f). The maximum inhibition zone was formed for 0.07AgNPs against *Pseudomonas aeruginosa* as 36 ± 0.23 mm. The strong activities can be ascribed to many factors working simultaneously such as the uniform dispersion of nanoparticles over the surface of the membrane. The interfacial interactions between silver atoms and g-C_3N_4 also supported the excellent antibacterial activity [19,54]. Concluding from the above reported results and acknowledging the bacteria-killing properties of chitosan/vanillin/GCN/AgNPs it can be proposed that these membranes could be utilized efficiently in wound dressing applications [55].

The *in-vitro* drug release behavior of AgNPs loaded polymeric composites were studied using three different fluids *i.e.*, distilled water, normal saline and simulated wound fluid (Table S3 in Supporting information). For a demonstration of drug release, optimized composite membrane CGN-3 was used owing to its excellent swelling ability, gel fraction, oxygen permeability, porosity, water vapor transmission rate, mechanical properties and good anti-bacterial properties. The release of nanoparticles started within 30 min in fluid attributed to the rapid diffusion of AgNPs embedded near-surface. The release started rapidly; however, it slowed down over the period of time. The sudden release was not observed leading to the conclusion that NPs were cross-linked effectively. The interactions of NPs with polymeric materials could be another possible reason. The maximum release was noticed in swollen states of composite membranes. The released drug from specimen was just a fraction of the incorporated drug, so it is safe to predict that the remaining AgNPs were still loaded inside due to physical interactions between starch, chitosan and NPs. Following models were used to assess the kinetic of hydrogen membrane: zero-order model, first-order model, Hixon-Crowell model, Higuchian model and Korsmeyer-peppas model. The highest value of regression coefficient (R^2) was chosen as criteria for the best fit model. The compared R^2 values shown that the best model fit for AgNPs release is Higuchi model with values 0.953, 0.976 and 0.983 for water, salt and simulated wound fluid respectively as discussed in other report. To confirm the mechanism of drug release from polymeric composites, after confirmation from Higuchi model, the Korsmeyer Peppas method was employed. The results confirmed that the release mechanism of nanoparticles from the membrane is through "non-fickian diffusion". The claim is justified from the 'n' value from the Korsmeyer Peppas equation. All values were found to be higher than 0.5 that confirms the anomalous drug release mechanism of fabricated hydrogels.

In conclusion, this study presented the successful fabrication of chitosan/vanillin/GCN/AgNPs. After the development of hydrogel different characterization techniques were performed to assess the properties. FT-IR and XRD confirm the successful fabrication and incorporation of graphitic carbon nitride and starch caped silver nanoparticles in composite membranes. The addition of g-C_3N_4 and starch-caped silver nanoparticles enhanced the mechanical strength of composite membrane up to 25.9 ± 0.24 MPa. The fabricated hydrogels have shown excellent antibacterial activity against *S. aureus* and *Pseudomonas aeruginosa* with a maximum zone of inhibitions 30 ± 0.25 mm and 36.23 ± 0.23 mm respectively. Furthermore, the synthesized membranes showed great swelling properties against water, salt, blood and simulated wound fluid. The composite also demonstrated good moisture retention capability which favors wound dressing materials. Gel fraction values confirmed the effectiveness of vanillin as a crosslinker. Good oxygen permeability results proved the breathable nature of fabricated membranes, as nutrients and oxygen exchange are necessary in biomedical applications. *In vitro* release results showed the sustained release of nanoparticles from polymer matrix following Higuchi model. The results encouraged and envisaged the potential of these membranes to be effectively used as wound dressing materials, skin regeneration and load bearing scaffolds.

Declaration of competing interest

The authors declare that they have no known competing financial interests or personal relationships that could have appeared to influence the work reported in this paper.

Acknowledgments

This work was supported by the National Natural Science Foundation of China (No. 52003113), Guangdong Basic and Applied Basic Research Foundation (Nos. 2021A1515010745, 2020A1515110356), and Science and Technology Projects of Guangzhou City (No. 202102020359). Y.C. Gan thanks the financial support from the China Postdoctoral Science Foundation (No. F121280003).

Supplementary material

Supplementary material associated with this article can be found, in the online version, at doi:10.1016/j.cclet.2022.108071.

References

[1] P.P. Kalelkar, M. Riddick, A.J. García, Nat. Rev. Mater. 7 (2022) 39–54.
[2] C. Cai, T. Wang, X. Han, et al., Chin. Chem. Lett. 33 (2022) 1963–1969.
[3] M. Zhang, X. Zhao, Int. J. Biol. Macromol. 162 (2020) 1414–1428.
[4] P. Deng, W. Jin, Z. Liu, M.Y. Gao, J.P. Zhao, Carbohydr. Polym. 260 (2021) 117767.
[5] A. Pellicoro, P. Ramachandran, J.P. Iredale, J.A. Fallowfield, Nat. Rev. Immunol. 14 (2014) 181–194.
[6] X. Zhao, B. Guo, H. Wu, Y. Liang, P.X. Ma, Nat. Commun. 9 (2018) 2784.
[7] Y. Dong, H. Hong, L. Xu, et al., Chin. Chem. Lett. 21 (2010) 1011–1014.
[8] T. Hasing, H. Tang, M. Brym, et al., Nat. Food 1 (2020) 811–819.
[9] G. Zhou, A. Ruhan, H. Ge, et al., Burns 40 (2014) 1668–1678.
[10] J. Sánchez-Laínez, B. Zornoza, C. Téllez, J. Coronas, J. Mater. Chem. A 4 (2016) 14334–14341.
[11] L. Huang, C. Li, W. Yuan, G. Shi, Nanoscale 5 (2013) 3780–3786.
[12] F.F. An, X.H. Zhang, Theranostics 7 (2017) 3667–3689.
[13] F. Li, H. Hou, J. Yin, X. Jiang, Sci. Adv. 4 (2018) eaar5762.
[14] W.J. Ong, L.L. Tan, Y.H. Ng, Y. Ng, S.T. Yong, Chem. Rev. 116 (2016) 7159–7329.
[15] S. He, J. Wang, M. Yu, et al., Polymers (Basel) 11 (2019) 610.
[16] G. Liao, F. He, Q. Li, et al., Prog. Mater. Sci. 112 (2020) 100666.
[17] A.L. Urzedo, M.C. Goncalves, M.H.M. Nascimento, et al., ACS Biomater. Sci. Eng. 6 (2020) 2117–2134.
[18] Y. Li, Y. Chang, X. Lian, et al., J. Biomed. Nanotechnol. 14 (2018) 1515–1542.
[19] A. Ahmed, M.B.K. Niazi, Z. Jahan, et al., Eur. Polym. J. 130 (2020) 109650.
[20] N. Vahedi-Notash, M.M. Heravi, A. Alhampour, P. Mohammadi, Sci. Rep. 10 (2020) 19322.
[21] A. Hebeish, T.I. Shaheen, M.E.El. Naggar, Int. J. Biol. Macromol. 87 (2016) 70–76.
[22] X. Feng, D. Li, J. Han, X. Zhuang, J. Ding, Mater. Sci. Eng. C 76 (2017) 1121–1128.
[23] M.M. Iftime, S. Moria, L. Marin, Carbohydr. Polym. 165 (2017) 39–50.
[24] D. Cao, Y. Zhang, Z. Cui, et al., Mater. Sci. Eng. C 70 (2017) 665–672.
[25] J. Hu, Z. Wang, J.M. Miszuk, et al., Carbohydr. Polym. 271 (2021) 118440.
[26] L. Wei, J. Lu, H. Xu, et al., Drug Discov. Today 20 (2015) 595–601.
[27] H. Gang, D. Lee, K.Y. Choi, et al., ACS Sustain. Chem. Eng. 5 (2017) 4582–4588.
[28] E. Hasanvand, A. Rafe, Int. J. Biol. Macromol. 131 (2019) 60–66.
[29] P.B. Ingabire, A. Haragirimana, Y. Liu, et al., J. Ind. Eng. Chem. 91 (2020) 213–222.
[30] E. Sharmin, M.T. Kafyah, A.A. Alzaydi, et al., Int. J. Biol. Macromol. 163 (2020) 2236–2247.
[31] Z. Wu, S. Tang, W. Deng, J. Luo, X. Wang, Food Chem. 363 (2021) 130342.
[32] M. Bahadoran, A. Shamloo, Y.D. Nokoorani, Sci. Rep. 10 (2020) 7342.
[33] X. Yang, Y. Tu, L. Li, S. Shang, X.M. Tao, ACS Appl. Mater. Interfaces 2 (2010) 1707–1713.
[34] R. Justin, B. Chen, Carbohydr. Polym. 103 (2014) 70–80.
[35] L. Fan, J. Yi, J. Tong, et al., Int. J. Biol. Macromol. 91 (2016) 358–367.
[36] R. Shapi'i, S.H. Othman, Int. Food. Res. J. 23 (2016) 187–193.
[37] M. Salari, M.S. Khiabani, R.R. Mokarram, B. Ghanbarzadeh, H.S. Kafil, Food Hydrocoll 84 (2018) 414–423.
[38] T. Khampieng, S. Wongkittithavorn, S. Chaiarwut, et al., J. Drug. Deliv. Sci. Technol. 44 (2018) 91–100.
[39] V. Vatanpour, S. Faghani, R. Keyikoglu, A. Khataee, Carbohydr. Polym. 256 (2021) 117413.
[40] C. Talodthaisong, W. Boonta, S. Thammawithan, et al., Mater. Today Commun. 24 (2020) 100992.
[41] F. Yokoyama, I. Masada, K. Shimamura, T. Ikawa, K. Monobe, Colloid Polym. Sci. 264 (1986) 595–601.
[42] Y. Xie, X. Liao, J. Zhang, F. Yang, Z. Fan, Int. J. Biol. Macromol. 119 (2018) 402–412.
[43] B. Tyliszczak, A. Drabczyk, S. Kudłacik-Kramarczyk, et al., Biointerfaces 160 (2017) 325–330.
[44] X. Li, B. Cho, R. Martin, et al., Sci. Transl. Med. 11 (2019) eaau6210.
[45] G.D. Winter, Nature 193 (1962) 293–294.
[46] S. Wittaya-areekul, C. Prahsarn, Int. J. Pharm. 313 (2006) 123–128.
[47] B.F. Achachlouei, Y. Zahedi, Carbohydr. Polym. 199 (2018) 415–425.
[48] M. Zhang, G. Wang, D. Wang, et al., Int. J. Biol. Macromol. 175 (2021) 481–494.
[49] A. Çay, M. Miraftab, E.P.A. Kumbasar, Eur. Polym. J. 61 (2014) 253–262.
[50] C. Zhang, Y. Zhou, L. Zhang, et al., Int. J. Mol. Sci. 19 (2018) 3330.
[51] S.S. Biranje, P.V. Madiwale, K.C. Patankar, et al., Int. J. Biol. Macromol. 121 (2019) 936–946.
[52] D. Zhang, W. Zhou, B. Wei, et al., Carbohydr. Polym. 125 (2015) 189–199.
[53] M.S. Sarwar, M.B.K. Niazi, Z. Jahan, et al., Carbohydr. Polym. 184 (2018) 453–464.
[54] H. Ye, J. Cheng, K. Yu, Int. J. Biol. Macromol. 121 (2019) 633–642.
[55] C. Liu, H. Shen, S. Wang, et al., Chin. Chem. Lett. 29 (2018) 1824–1828.